

## Important Notice to Authors

Attached is a PDF proof of your forthcoming article in PRB. Your article has 8 pages and the Accession Code is **BP12960**.

Please note that as part of the production process, APS converts all articles, regardless of their original source, into standardized XML that in turn is used to create the PDF and online versions of the article as well as to populate third-party systems such as Portico, Crossref, and Web of Science. We share our authors' high expectations for the fidelity of the conversion into XML and for the accuracy and appearance of the final, formatted PDF. This process works exceptionally well for the vast majority of articles; however, please check carefully all key elements of your PDF proof, particularly any equations or tables.

Figures submitted electronically as separate PostScript files containing color appear in color in the online journal. However, all figures will appear as grayscale images in the print journal unless the color figure charges have been paid in advance, in accordance with our policy for color in print (<http://journals.aps.org/authors/color-figures-print>).

**No further publication processing will occur until we receive your response to this proof.**

### Specific Questions and Comments to Address for This Paper

- 1 Please check changes made throughout to ensure correct representation and meaning are preserved.
  - 2 Please check changes to author names used in textual reference citations throughout made to match order and/or spelling of author names used in each reference.
  - 3 The .eps files for Fig. 2(b), (c) do not match the ones in the PDF you supplied. Please confirm that the correct figures were used.
  - 4 In the sentence beginning with "The plane...", please verify end of sentence, or is something missing?
  - 5 Please note that claims of priority usually are discouraged. Therefore, in the sentence beginning with "As a result,..." please check changes made to ensure meaning is preserved.
  - 6 Please verify new and run-in paragraphs directly following displayed equations throughout to ensure meaning is preserved.
  - 7 In the sentence beginning with "As expected,..." and throughout, please verify that " $\vec{b}$ " is meant, or is " $\vec{b}$ " or "**b**" intended?
  - 8 In the sentence beginning with "These two..." please verify change from "Hirth and Lothe [23]" to "Hirth and Lothe [25]."
  - 9 Please verify all information for Reference [28].
- Q: This reference could not be uniquely identified due to incomplete information or improper format. Please check all information and amend if applicable.

**Open Funder Registry:** Information about an article's funding sources is now submitted to Crossref to help you comply with current or future funding agency mandates. Crossref's Open Funder Registry (<http://www.crossref.org/fundingdata/>) is the definitive registry of funding agencies. Please ensure that your acknowledgments include all sources of funding for your article following any requirements of your funding sources. Where possible, please include grant and award ids. Please carefully check the following funder information we have already extracted from your article and ensure its accuracy and completeness:

U.S. Department of Energy's, DE-AC04-94AL85000

### Other Items to Check

- Please note that the original manuscript has been converted to XML prior to the creation of the PDF proof, as described above. Please carefully check all key elements of the paper, particularly the equations and tabular data.
- Title: Please check; be mindful that the title may have been changed during the peer review process.
- Author list: Please make sure all authors are presented, in the appropriate order, and that all names are spelled correctly.
- Please make sure you have inserted a byline footnote containing the email address for the corresponding author, if desired. Please note that this is not inserted automatically by this journal.
- Affiliations: Please check to be sure the institution names are spelled correctly and attributed to the appropriate author(s).
- Receipt date: Please confirm accuracy.
- Acknowledgments: Please be sure to appropriately acknowledge all funding sources.
- Hyphenation: Please note hyphens may have been inserted in word pairs that function as adjectives when they occur before a noun, as in "x-ray diffraction," "4-mm-long gas cell," and "R-matrix theory." However, hyphens are deleted from word pairs when they are not used as adjectives before nouns, as in "emission by x rays," "was 4 mm in length," and "the R matrix is tested."

Note also that Physical Review follows U.S. English guidelines in that hyphens are not used after prefixes or before suffixes: superresolution, quasiequilibrium, nanoprecipitates, resonancelike, clockwise.

- Please check that your figures are accurate and sized properly. Make sure all labeling is sufficiently legible. Figure quality in this proof is representative of the quality to be used in the online journal. To achieve manageable file size for online delivery, some compression and downsampling of figures may have occurred. Fine details may have become somewhat fuzzy, especially

in color figures. The print journal uses files of higher resolution and therefore details may be sharper in print. Figures to be published in color online will appear in color on these proofs if viewed on a color monitor or printed on a color printer.

- Please check to ensure that reference titles are given as appropriate.
- Overall, please proofread the entire *formatted* article very carefully. The redlined PDF should be used as a guide to see changes that were made during copyediting. However, note that some changes to math and/or layout may not be indicated.

### **Ways to Respond**

- **Web:** If you accessed this proof online, follow the instructions on the web page to submit corrections.
- **Email:** Send corrections to [prbproofs@aptaracorp.com](mailto:prbproofs@aptaracorp.com)  
Subject: **BP12960** proof corrections
- **Fax:** Return this proof with corrections to +1.703.791.1217. Write **Attention:** PRB Project Manager and the Article ID, **BP12960**, on the proof copy unless it is already printed on your proof printout.
- **Mail:** Return this proof with corrections to **Attention:** PRB Project Manager, Physical Review B, c/o Aptara, 3110 Fairview Park Drive, Suite #900, Falls Church, VA 22042-4534, USA.

**Atomistic calculations of dislocation core energy in aluminium**X. W. Zhou,<sup>1,\*</sup> R. B. Sills,<sup>2</sup> D. K. Ward,<sup>3</sup> and R. A. Karnesky<sup>4</sup><sup>1</sup>*Mechanics of Materials Department, Sandia National Laboratories, Livermore, California 94550, USA*<sup>2</sup>*Gas Transfer Systems Department, Sandia National Laboratories, Livermore, California 94550, USA*<sup>3</sup>*Radiation and Nuclear Detection Materials and Analysis Department, Sandia National Laboratories, Livermore, California 94550, USA*<sup>4</sup>*Hydrogen and Materials Science Department, Sandia National Laboratories, Livermore, California 94550, USA*

(Received 29 February 2016; revised manuscript received 23 January 2017; published xxxxxx)

A robust molecular-dynamics simulation method for calculating dislocation core energies has been developed. This method has unique advantages: It does not require artificial boundary conditions, is applicable for mixed dislocations, and can yield converged results regardless of the atomistic system size. Utilizing a high-fidelity bond order potential, we have applied this method in aluminium to calculate the dislocation core energy as a function of the angle  $\beta$  between the dislocation line and the Burgers vector. These calculations show that, for the face-centered-cubic aluminium explored, the dislocation core energy follows the same functional dependence on  $\beta$  as the dislocation elastic energy:  $E_c = A\sin^2\beta + B\cos^2\beta$ , and this dependence is independent of temperature between 100 and 300 K. By further analyzing the energetics of an extended dislocation core, we elucidate the relationship between the core energy and the core radius of a perfect versus an extended dislocation. With our methodology, the dislocation core energy can accurately be accounted for in models of dislocation-mediated plasticity.

DOI: [10.1103/PhysRevB.00.004100](https://doi.org/10.1103/PhysRevB.00.004100)**I. INTRODUCTION**

With low hydrogen solubility and a high strength-to-weight ratio, aluminium alloys are attractive for both hydrogen energy and transportation applications, respectively, that require high resistance to hydrogen embrittlement and light weight. Dislocation dynamics (DD) simulations [1] provide a tool for studying the mechanical properties of metals and alloys. One key input for DD simulations that is often overlooked is the core energy of dislocation lines and its variation with the character angle  $\beta$  formed between the line and the Burgers vector. The core energy contributes to the dislocation line tension and alters the behavior of dislocation lines as they bow out to bypass obstacles and react to form junctions. Unfortunately, dislocation cores cannot be described by linear elasticity theory, and hence their study requires a computational tool with atomistic resolution. Despite the pioneering work by Cai *et al.* [2,3] and Li *et al.* [4], much remains poorly understood concerning the nature of dislocation cores and their energies.

Dislocation core energies can be calculated using quantum-mechanical or empirical atomistic simulations under continuum [5–8], free [9], or periodic [1–4,10–15] boundary conditions. Continuum boundary conditions are challenging to use when dislocation configurations are unknown *a priori*, such as in face-centered-cubic (fcc) metals, such as aluminium where perfect dislocations dissociate into partial dislocations separated by a stacking fault. Periodic boundary conditions usually are implemented using a so-called quadruple dislocation configuration [10] where positive and negative dislocations (lying in  $z$ ) alternate in sign in both the  $x$  and the  $y$  directions so that a negative dislocation can recover the crystal periodicity destroyed by the preceding positive dislocation in both  $x$  and  $y$  directions. Although the quadruple configuration requires an orthorhombic computational cell to include four dislocations, it can be replicated with a nonorthorhombic cell containing only two dislocations [10,16]. A potential difficulty

with this method is that, because positive and negative dislocations are on the same slip plane ( $x$  direction), they can glide and annihilate. This configuration cannot be used unless a barrier, such as the Peierls stress is sufficiently strong to pin the dislocations in place. A more general dislocation configuration that enables an offset of dislocations on different slip planes may solve this problem [2–4,16]. Dislocation core energies of aluminium have also been calculated using the generalized stacking fault energy obtained from density functional theory [17]. Because core relaxation is not treated directly in this model, however, it is unclear how this method compares with the direct atomistic simulation approach.

Recently, we have used molecular dynamics (MD) to calculate core energies of edge dislocations under periodic boundary conditions [18]. In our approach, we eliminate the alternation of dislocations in  $x$ , which prevents annihilation by glide. The purpose of the present paper is threefold: (a) Further extend this method to mixed dislocations and generate a complete set of aluminium dislocation core energies over the full range of possible character angles; (b) establish a generic analytical equation for the dislocation core energy in aluminium; and (c) further our understanding of the physics of dislocation cores in fcc metals. For our calculations, we utilize a high-fidelity Al-Cu bond order potential [19].

**II. METHODS**

The overall approach we will use for computing the core energy is similar to the other methods discussed above. Using atomistic simulations, we will compute the total energy per unit length of dislocation  $\Gamma$  of a multipolar dislocation system. This line energy can be expressed in terms of two contributions as

$$\Gamma(\beta) = E_c(\beta) + E_{el}(\beta), \quad (1)$$

where  $E_c$  and  $E_{el}$ , respectively, are the core and elastic energies per unit length of the dislocation and  $\beta$  is the character angle. Using elasticity theory, the elastic energy can be computed analytically in isotropic theory (see the

\*xzhou@sandia.gov

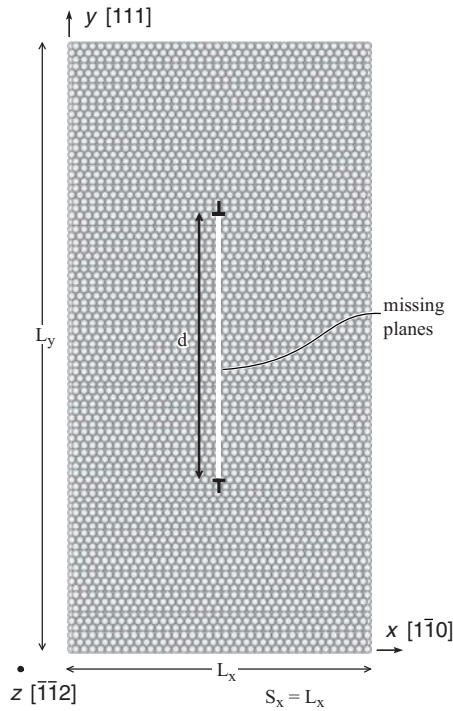


FIG. 1. Geometry for  $\beta = 90^\circ$  (edge) dislocation dipoles (dislocation spacing  $S_x$  equals system dimension  $L_x$ ).

89 Appendix) and numerically using anisotropic theory (using  
 90 the MADSUM code [2,20]), allowing for the core energy to  
 91 be uniquely determined from MD simulations for a given  
 92 character angle. We use both isotropic and anisotropic  
 93 theories for these calculations. This is because most discrete  
 94 dislocation dynamics codes use isotropic theory to compute  
 95 dislocation interactions and the analytical expressions of  
 96 isotropic theory allow us to rationalize our results.

#### A. Edge dislocations ( $\beta = 90^\circ$ )

98 The geometry of the method for edge dislocations is shown  
 99 in Fig. 1. The system has dimensions of  $L_x$ ,  $L_y$ , and  $L_z$  in the  $x$ ,  
 100  $y$ , and  $z$  directions, respectively. When the system is aligned in  
 101 the  $[1\bar{1}0]$   $x$  and  $[111]$   $y$  directions, an edge dislocation dipole  
 102 with a Burgers vector  $[1\bar{1}0]a/2$  and a dislocation line parallel to  
 103 the  $[\bar{1}\bar{1}2]z$  direction can be created by removing a  $(1\bar{1}0)$  plane  
 104 or equivalently two  $(2\bar{2}0)$  planes as indicated by the white  
 105 line in Fig. 1. The height of the dipole  $d$  equals the height of  
 106 the missing planes. Under periodic boundary conditions, the  
 107 dislocations form an infinite array along  $x$  and  $y$ . Each dislocation  
 108 has infinite length in the  $z$  direction, and the dislocation  
 109 spacing in the  $x$  direction  $S_x$  equals the system dimension  $L_x$ .

110 Using this atomistic configuration, we compute the total energy  
 111 of the system with and without a dislocation dipole present  
 112 using time-averaged MD simulations (discussed below). Note  
 113 that the number of atoms in the dislocation-containing system  
 114  $N_d$  may not equal the number of atoms in the dislocation-free  
 115 system  $N_0$  due to the missing planes of the edge component  
 116 of dislocations. Fortunately, each atom in the dislocation-free  
 117 system is identical, and as a result, the energy of the  
 118 dislocation-free system can be scaled by a factor of  $N_d/N_0$

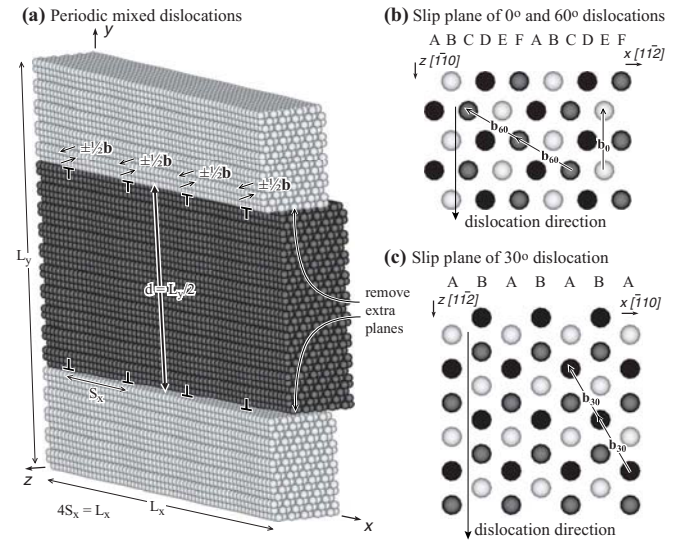


FIG. 2. Geometry for screw and mixed dislocations: (a) Three-dimensional configuration, (b) top view of  $\beta = 0^\circ$  (screw) and  $\beta = 60^\circ$  (mixed) dislocation slip plane, and (c) top view of  $\beta = 30^\circ$  dislocation slip plane.

to match the number of atoms in the dislocation-containing  
 119 system. Under this condition, the energy due to the dipole array  
 120 is the difference in the energies (after the scaling) between  
 121 these two configurations. As shown in the Appendix, the dipole  
 122 array energy can be expressed analytically using isotropic  
 123 linear elasticity theory for a chosen core radius  $r_0$ . As discussed  
 124 in Sec. III C, fitting the MD data to this analytical equation then  
 125 allows us to determine the core energy [18].  
 126

#### B. Screw ( $\beta = 0^\circ$ ) and mixed dislocations ( $0^\circ \leq \beta < 90^\circ$ )

127 The method described above cannot be applied to screw  
 128 and mixed dislocations because the shear deformation of the  
 129 screw component destroys the crystal periodicity. As shown  
 130 in Fig. 2(a), if the dipole distance is exactly half of the system  
 131 dimension, i.e.,  $d = L_y/2$ , we can always create a dislocation  
 132 dipole symmetrically as long as the two half regions (the dark  
 133 and light regions) are displaced equally by  $\pm \frac{1}{2}\mathbf{b}$ . Note that we  
 134 found this symmetrical condition necessary to ensure the correct  
 135 results. By then introducing multiple dislocation dipoles,  
 136 we can always satisfy periodic boundary conditions; however,  
 137 the number of dipoles necessary depends on the character angle  
 138 of the dislocation lines. As an example, Fig. 2(b) shows a com-  
 139 mon slip plane for  $\beta = 0^\circ$  (screw) and  $60^\circ$  dislocations where  
 140 the dislocation line aligns with  $z[\bar{1}10]$ , the screw Burgers vec-  
 141 tor of  $\mathbf{b}_0 = [1\bar{1}0]a/2$  forms a  $\beta = 180^\circ$  (or equivalently  $\beta =$   
 142  $0^\circ$ ) angle, and the  $\beta = 60^\circ$  Burgers vector of  $\mathbf{b}_{60} = [0\bar{1}1]a/2$   
 143 forms a  $\beta = 120^\circ$  (or equivalently  $\beta = 60^\circ$ ) angle. The plane  
 144 stacking in the  $x[11\bar{2}]$  direction is  $ABCDEFABCDEF\dots$ . It  
 145 can be seen that an arbitrary  $C$  plane can recover to another  
 146  $C$  plane if it is shifted by  $2\mathbf{b}_{60}$ . Hence, periodic boundary  
 147 conditions can be maintained for the  $\beta = 60^\circ$  dislocation if  
 148 we create four dislocation dipoles in the computational cell  
 149 as shown in Fig. 2(a). Likewise, an arbitrary  $E$  plane can  
 150 recover to another  $E$  plane if it is shifted by  $\mathbf{b}_0$ . Hence, periodic  
 151 boundary conditions can be used for the screw dislocation if we  
 152

153 create two dislocation dipoles. Similarly, the  $\beta = 30^\circ$  dislocation  
 154 shown in Fig. 2(c) can also be simulated under periodic  
 155 boundary conditions by creating four dislocation dipoles per  
 156 cell. Using similar arguments, the character angles  $10.89^\circ$ ,  
 157  $19.11^\circ$ ,  $40.89^\circ$ ,  $49.11^\circ$ ,  $70.89^\circ$ , and  $79.11^\circ$  can be simulated  
 158 using 28 dislocation dipoles. These observations allow our  
 159 method to be extended to screw and mixed dislocations.

160 The approach described above requires adding more dislo-  
 161 cation to the simulation cell, causing the size of the atomistic  
 162 system to increase. With this approach, all simulation cells are  
 163 orthorhombic. Although it is possible to reduce the number of  
 164 dislocations by making the axes of the cell nonorthorhombic  
 165 [1], we have opted for orthorhombic cells because there is  
 166 less possibility for artifacts due to improper enforcement of  
 167 periodicity and/or pressure-free boundary conditions.

### 168 C. Time-averaged MD simulations

169 We have found that, although molecular statics (MS) energy  
 170 calculations based on the conjugate gradient method can give  
 171 low relative errors, they produce large total errors that increase  
 172 as the system dimension increases [18]. This is not satisfactory  
 173 for calculating dislocation energies, which are related to total  
 174 energies of (dislocated and perfect) systems if the length along  
 175 dislocation is fixed. Time-averaged properties of long-time  
 176 MD simulations, on the other hand, are found to converge  
 177 satisfactorily regardless of the system dimensions [18]. This  
 178 sounds surprising at a first sight but can be understood because  
 179 the time-averaged MD calculations not only average out the  
 180 thermal noises, but also are analogous to performing ensemble  
 181 averages of many MS simulations with different perturbations  
 182 of initial configurations. Additionally, MS pertains only to 0 K  
 183 whereas finite temperature effects are incorporated in MD.  
 184 Moreover, finite temperature systems are less likely to become  
 185 trapped in metastable states, making them more robust for  
 186 determining the minimum energy core configuration.

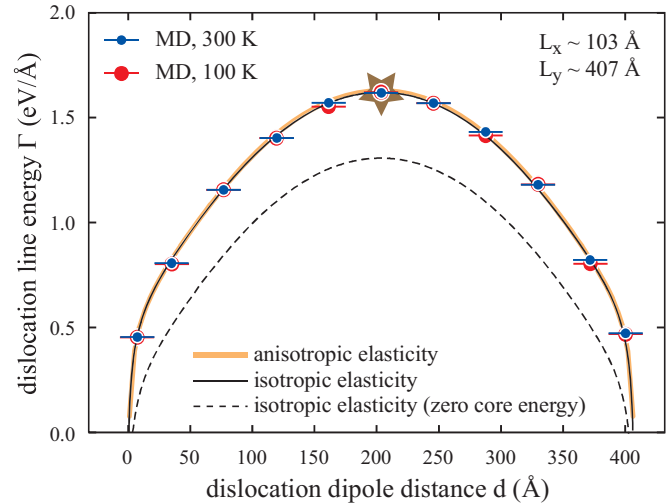
187 The majority of our simulations are performed at 300 K  
 188 whereas selected other temperatures also are used to explore  
 189 the temperature effects. All properties presented in this paper  
 190 are time averaged from 4-ns MD simulations using a time  
 191 step of 0.004 ps. After discarding the first 0.8 ns to allow for  
 192 equilibration, the system energy and dimension are averaged  
 193 over all the time steps for the remaining 3.2 ns. Unless  
 194 otherwise indicated, our simulations use a zero pressure  
 195  $N$ - $P$ - $T$  (constant number of atoms, pressure, and temperature)  
 196 ensemble with the dimension in the dislocation line direction  
 197 ( $z$ ) further fixed to match the plane strain assumption used in  
 198 the classical dislocation theories. We also perform simulations  
 199 that allow the  $z$  dimension to change but the same results are  
 200 obtained as will be shown below. MD code LAMMPS [21,22] is  
 201 used for all of our simulations.

## 202 III. RESULTS AND DISCUSSION

### 203 A. Edge dislocations ( $\beta = 90^\circ$ )

204 Two series of simulations are performed. In the first  
 205 series, the crystal contains 72 ( $2\bar{2}0$ ) planes in  $x$ , 174 (111)  
 206 planes in  $y$ , 30 ( $\bar{2}\bar{2}4$ ) planes in  $z$ , and the dislocation dipole  
 207 distance  $d$  varies from 3 to 171 (111) planes. The same  
 208 series of simulations are repeated for both 300- and 100-K

(a) Effect of dislocation dipole distance  $d$



(b) Effect of dislocation spacing  $S_x (= L_x)$

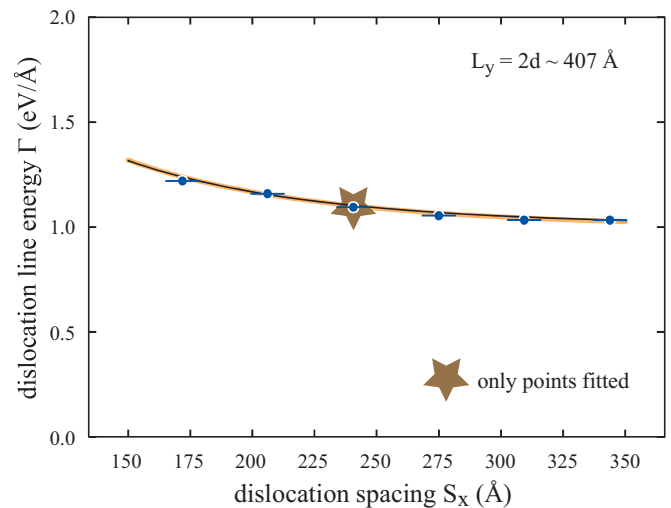


FIG. 3. Edge dislocation line energy as a function of (a) disloca-  
 tion dipole distance  $d$  and (b) dislocation spacing  $S_x (= L_x)$ . Error  
 bars represent the standard deviation of MD data. Note that in (a), the  
 solid and dashed lines differ only by the constant core energy.

209 temperatures. The resulting total dislocation line energies  
 210 (including both the core and the elastic energies) and their  
 211 standard deviation are shown as a function of the dipole height  
 212 in Fig. 3(a). The thin black solid line in the figure corresponds  
 213 to an isotropic fit to few representative MD data (marked by the  
 214 brown stars in both Figs. 3 and 4) using Eq. (A1) after selecting  
 215 an appropriate core radius of  $r_0 = 10$  Å. Additionally, we show  
 216 the fit using anisotropic elasticity theory (with  $C_{11} = 118.4$ ,  
 217  $C_{12} = 62.6$ , and  $C_{44} = 33.5$  GPa<sup>1</sup>) as a thick orange solid line.

<sup>1</sup>These elastic constants differ slightly from the 0 K constants  
 of the interatomic potential ( $C_{11} = 114.9$ ,  $C_{12} = 62.6$ , and  $C_{44} =$   
 $31.6$  GPa). We used slightly different values in order to achieve an  
 optimal fit with the MD results which were obtained at 300 K.

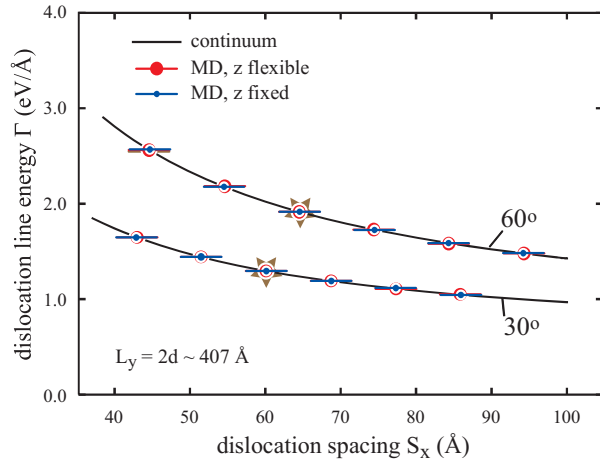
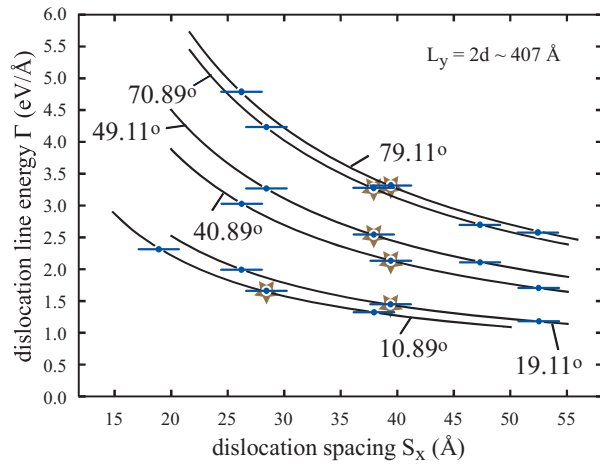
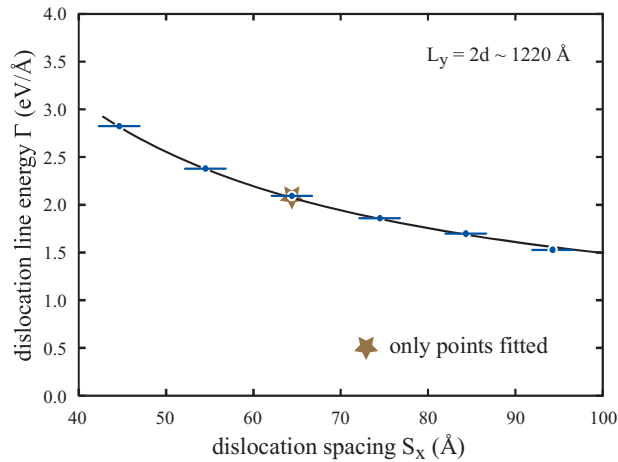
**(a)** 30°, 60° dislocations

**(b)** 10.89°, 19.11°, 40.89°, 49.11°, 70.89°, 79.11° dislocations

**(c)** 0.0° (screw) dislocation


FIG. 4. Line energies as a function of dislocation spacing  $S_x$  for (a) 30° and 60°, (b) 10.89°, 19.11°, 40.89°, 49.11°, 70.89°, and 79.11°, and (c) 0° dislocations. Error bars represent the standard deviation of MD data.

It can be seen from Fig. 3(a) that the statistical errors of all of our MD data are near zero within the numerical resolution demonstrated in the figure. A related consequence of the zero errors is that all of our MD data fall right on top of the continuum line, despite the fact that many MD data are not used in the fitting. This strongly validates our MD approach for calculating dislocation energies, which also corroborates well our derived isotropic continuum expressions for periodic dislocation arrays Eqs. (A1)–(A5) in the Appendix. Interestingly, the isotropic curve matches the anisotropic curve perfectly, justifying the validity of the isotropic approach for aluminium analysis. One important observation from Fig. 3(a) is that the temperature does not impact the core energy. This is because differences in entropies and thermal energies between perfect and dislocated systems are both negligible [23].

For reference, the thin black dashed line in Fig. 3(a) is the isotropic continuum result without the constant core energy. The difference between the thin dashed and the solid lines, corresponding to the constant core energy, is a significant fraction of the overall line energy for the range of dipole configurations considered. Clearly the error caused by ignoring the core energy is significant, demonstrating that our approach is a sensitive method for studying dislocation energies.

Figure 3(a) shows that the dislocation energies are symmetric with respect to dipole height  $d$ . This is because when  $d$  goes to zero, the dislocations in the dipole annihilate, leading to a low energy. When  $d$  is large (close to  $L_y$ ), dislocations and their other dipole counterparts (periodic images) also annihilate, leading to a low energy. Capturing this phenomenon is one strong validation of our MD data.

The second series of simulations examines the dislocation energy as a function of the lateral spacing  $S_x$  of the dislocation dipoles. For this series, the crystal contains 174 (111) planes in  $y$ , 30 ( $\bar{2}24$ ) planes in  $z$ , the dislocation dipole distance  $d$  equals 87 (111) planes, and the  $x$  dimension of the system varies from 120 to 240 ( $\bar{2}20$ ) planes. The same method is used to calculate the dislocation energies. The corresponding results are shown in Fig. 3(b) as a function of dislocation lateral spacing  $S_x (= L_x)$ . Again, Fig. 3(b) indicates that the MD results fit the continuum model (both isotropic and anisotropic) very well.

**B. Mixed ( $0^\circ \leq \beta \leq 90^\circ$ ) and screw ( $\beta = 0^\circ$ ) dislocations**

Mixed dislocations with regular angles  $\beta = 60^\circ$  and  $30^\circ$  and nonregular angles  $\beta = 10.89^\circ$ ,  $19.11^\circ$ ,  $40.89^\circ$ ,  $49.11^\circ$ ,  $70.89^\circ$ , and  $79.11^\circ$ , as well as the screw dislocation with  $\beta = 0^\circ$ , are all studied. For  $\beta = 60^\circ$ , the crystal contains 174 (111) planes in  $y$ , 16 ( $\bar{2}20$ ) planes in  $z$ , the dislocation dipole distance  $d$  equals 87 (111) planes, and the  $x$  dimension of the system varies from 216 to 456 ( $\bar{2}24$ ) planes. For  $\beta = 30^\circ$ , the crystal contains 174 (111) planes in  $y$ , 30 ( $\bar{2}24$ ) in  $z$ ,  $d$  equals 87 (111) planes, and the  $x$  dimension varies from 120 to 240 ( $\bar{2}20$ ) planes. Four dislocation dipoles are created in the computational cell as shown in Fig. 2(a) so that the lateral dislocation spacing  $S_x$  equals  $L_x/4$ . The crystals used for dislocations with  $\beta = 10.89^\circ$ ,  $49.11^\circ$ , and  $70.89^\circ$  contain 174 (111) planes in  $y$ ,  $54 \left(\frac{9}{7} \frac{36}{7} - \frac{45}{7}\right)$  planes in  $z$ , 87 (111) planes for the dislocation dipole height  $d$ , and various  $x$  dimensions from 1050 to 2625 ( $-\frac{45}{7} \frac{30}{7} \frac{15}{7}$ ) planes. The only difference among the  $10.89^\circ$ ,  $49.11^\circ$ , and  $70.89^\circ$  dislocations is that

218 We defer a discussion on the fitting process and the effects of  
219 the core radius until later.

they have different Burger vectors  $\mathbf{b} = [01\bar{1}]a/2$ ,  $[\bar{1}01]a/2$ ,  
 and  $[\bar{1}10]a/2$ , respectively. For dislocations with  $\beta = 19.11^\circ$ ,  
 40.89°, and 79.11° angles, the crystals contain 174 (111)  
 planes in  $y$ , 45 ( $\frac{45}{7} - \frac{30}{7} - \frac{15}{7}$ ) planes in  $z$ , 87 (111) planes  
 for the dislocation dipole height  $d$ , and various  $x$  dimensions  
 from 1512 to 3024 ( $\frac{9}{7}\frac{36}{7} - \frac{45}{7}$ ) planes. The Burgers vectors  
 for the 19.11°, 40.89°, and 79.11° dislocations correspond to  
 $\mathbf{b} = [\bar{1}10]a/2$ ,  $[\bar{1}01]a/2$ , and  $[01\bar{1}]a/2$ , respectively. Unlike  
 the 60° and 30° regular angle dislocations, the nonregular  
 angles 10.89°, 19.11°, 40.89°, 49.11°, 70.89°, and 79.11°  
 require 28 dislocation dipoles to be used in the computational  
 cell to maintain periodic boundary conditions. As a result,  
 $S_x = L_x/28$ . Following the same method as described above,  
 total dislocation line energies are calculated as a function of  
 $S_x$ , and the results are shown in Fig. 4(a) for the regular angles  
 (30° or 60°) and in Fig. 4(b) for the nonregular angles. Again,  
 the MD results are very well characterized by the continuum  
 model.

The  $\beta = 0^\circ$  case imposes challenges for fcc metals due  
 to the annihilation of screw dislocations by cross slip. As a  
 result, the core energy of a screw dislocation in a fcc metal is  
 computed atomistically here. Through extensive iterations, we  
 find that when the  $y$  dimension is increased above 522 (111)  
 planes to reduce the attraction between opposite dislocations  
 and when the temperature is reduced below 10 K to trap  
 dislocations in metastable locations, the combination of both  
 conditions can prevent cross slip. Fortunately, the use of a low  
 temperature does not impact the results as has been shown  
 in Fig. 3(a). Hence, we perform simulations at 10 K for the  
 $\beta = 0^\circ$  case using crystals that contain 522 (111) planes in  $y$ ,  
 16 (2 $\bar{2}0$ ) planes in  $z$ , a dipole height  $d$  of 261 (111) planes,  
 and various  $x$  dimensions from 108 to 228 (2 $\bar{2}4$ ) planes. The  
 results obtained for the 0° dislocations are shown in Fig. 4(c).  
 Again, the data points fall right on top of the continuum line.

The MD simulations discussed above use a fixed  $z$  dimen-  
 sion assumed in the dislocation elastic theories (plane strain).  
 We have also performed similar MD simulations where the  
 $z$  dimension is allowed to relax, and the results are included  
 in Fig. 4(a). Interestingly, the flexible  $z$  condition produces  
 exactly the same results as the fixed  $z$  condition.

### C. Dislocation core energies

To compute the core energy using anisotropic theory, we  
 use the cubic elastic constants given above in conjunction  
 with the MADSUM code [2,20]. In the isotropic theory, the  
 continuum expression for the energy of periodic dislocation  
 arrays Eq. (A1) involves four parameters: dislocation core  
 radius  $r_0$ , core energy  $E_c$ , and elastic constants  $G$  and  $\nu$ .  
 These parameters can be obtained by fitting to the MD data.  
 However, the magnitude of the core radius  $r_0$  is not unique.  
 Conventionally, the only requirement for  $r_0$  is that any region  
 outside  $r_0$  satisfies linear elasticity theory. Obviously, there  
 exists a minimum value  $r_0^{\min}$  so that any  $r_0 \geq r_0^{\min}$  can be taken  
 as a valid core radius. This is because elasticity theory breaks  
 down very near the dislocation core, causing the elastic energy  
 to go to infinity as the core radius goes to zero. Hence, the core  
 radius must be large enough to exclude this unphysical region.  
 On the other hand, the core energy is really just a correction  
 to the linear elastic theory at a given reference core radius  $r_0$ .

TABLE I. Dislocation core energies  $E_c^{\text{iso}}$  and  $E_c^{\text{aniso}}$  (eV/Å)  
 obtained from isotropic and anisotropic elasticity theories for a core  
 radius of  $r_0 = 10$  Å.

| Dislocation angle $\beta$ | $E_c^{\text{iso}}$ | $E_c^{\text{aniso}}$ |
|---------------------------|--------------------|----------------------|
| 00.00°                    | 0.295              | 0.170                |
| 10.89°                    | 0.291              | 0.197                |
| 19.11°                    | 0.296              | 0.233                |
| 30.00°                    | 0.306              | 0.271                |
| 40.89°                    | 0.298              | 0.254                |
| 49.11°                    | 0.308              | 0.267                |
| 60.00°                    | 0.314              | 0.297                |
| 70.89°                    | 0.320              | 0.293                |
| 79.11°                    | 0.316              | 0.294                |
| 90.00°                    | 0.315              | 0.318                |

As a result, any value of  $r_0$  (including  $r_0 = 0$ ) can be taken as  
 a valid core radius if the core energy is allowed to be negative.  
 Here we define the minimum value  $r_0^{\min}$  so that any  $r_0 \geq r_0^{\min}$   
 will always lead to positive core energies for all values of  $\beta$ .  
 Through trial-and-error fitting,  $r_0^{\min}$  is determined to be 2.0 and  
 2.5 Å for isotropic and anisotropic theories, respectively.

Unlike the curves shown in Figs. 3 and 4 that are fitted  
 to few MD data points, we now fit all MD data to yield  
 the most precise fit. Table I shows our fitted dislocation  
 core energies with  $r_0 = 10$  Å obtained for different character  
 angles using both anisotropic and isotropic theories. Fits for  
 different core radii all result in identical isotropic elastic  
 constants of  $G = 0.1830$  eV/Å<sup>3</sup> (29.3 GPa) and  $\nu = 0.3874$ ,  
 very close to the values of  $G = 0.169$  eV/Å<sup>3</sup> (27 GPa) and  
 $\nu = 0.34$  commonly cited for aluminium [24],<sup>2</sup> confirming  
 the robustness of our results. Comparing the isotropic and  
 anisotropic core energies, we find that, despite the nearly  
 isotropic behavior of aluminium, the core energies predicted  
 by the two theories are different. For this value of the core  
 radius, anisotropic theory gives that the core energy varies by  
 nearly a factor of 2 from  $\beta = 0^\circ$  to 90° whereas in isotropic  
 theory the core energy is nearly independent of character angle.  
 Note, however, different core energies do not mean that the  
 two theories are inconsistent. In fact, the two theories yield  
 exactly the same total dislocation energies as shown in Fig. 3.  
 The differences just mean that the two theories have different  
 allocations of the total dislocation energies to the core and the  
 elastic components.

To reiterate, our results are strongly validated from numer-  
 ous aspects: (1) the convergence to a single core energy at  
 different dislocation spacings for a given character angle and  
 a given core radius, (2) the convergence to a single set of  
 isotropic elastic constants for all dislocation spacings, orien-  
 tations, and core radii, and (3) the strong match between MD  
 results and both the isotropic and the anisotropic continuum  
 results.

<sup>2</sup>Note that while aluminium is elastically anisotropic like most  
 crystalline solids, it exhibits a relatively weak anisotropy ratio of  
 $A = 1.2$  in both experiments [22] and our potential [19].

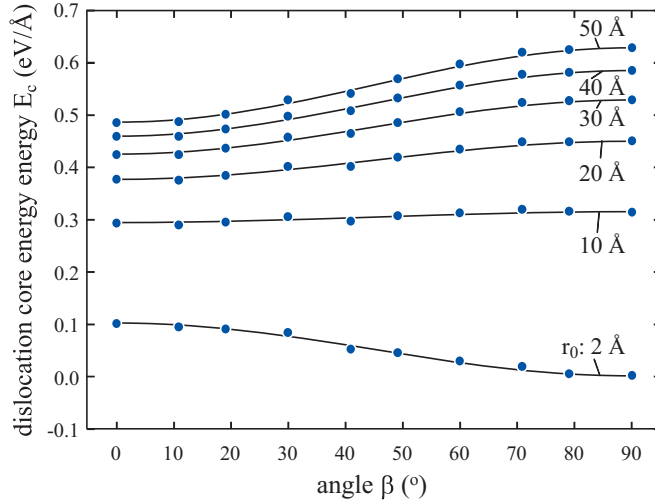


FIG. 5. Dislocation core energies as a function of dislocation angle  $\beta$  at different core radii  $r_0$ .

#### D. Analytical expression of core energy as a function of angle $\beta$

Using our MD results and isotropic elasticity theory, we can derive an analytical expression for the dislocation core energy at any character angle and with any core radius. To do so, we make the following assumption: Increases in the core energy as the core radius increases beyond the minimum core radius are due to elastic energy. Hence, the core energy can be written as

$$E_c(r_0, \beta) = E_c^{\text{ref}}(\beta) + \frac{Gb^2}{4\pi} \left( \cos^2 \beta + \frac{\sin^2 \beta}{1 - \nu} \right) \ln \frac{r_0}{r_0^{\text{ref}}}. \quad (2)$$

The first term is the core energy at a reference core radius  $r_0^{\text{ref}}$  ( $r_0^{\text{ref}} \geq r_0^{\text{min}}$ ), and the second term is the change in elastic energy attributed to the core upon changing the core radius from  $r_0^{\text{ref}}$  to  $r_0$  ( $r_0 \geq r_0^{\text{min}}$ ) [25]. Note that the same reasoning could be applied using anisotropic elasticity, however an analytical expression is not readily available. To complete this expression, we need to develop an analytical form for the core energy  $E_c^{\text{ref}}(\beta)$  at a chosen reference core radius  $r_0^{\text{ref}}$ . In principle,  $E_c^{\text{ref}}(\beta)$  should depend on crystal structure. For example, in body-centered-cubic materials, screw dislocations have nonplanar cores whereas edge dislocations have planar cores so that these two types of dislocations could have different core energies [26]. Examining our data, however, we find that the  $E_c^{\text{ref}}(\beta)$  can be expressed in the same form as the elastic energy [23],

$$E_c^{\text{ref}}(\beta) = A \sin^2 \beta + B \cos^2 \beta. \quad (3)$$

For example, if we choose a reference radius of  $r_0^{\text{ref}} = 30 \text{ \AA}$ , then the parameters  $A = 0.5294$  and  $B = 0.4528 \text{ eV/\AA}$ , which correspond to the edge and screw dislocation core energies, respectively, are derived from the MD simulations described above. In Fig. 5 we plot our core energy data for core radii of  $r_0 = 2, 10\text{--}50 \text{ \AA}$  with curves generated using Eqs. (2) and (3) at  $r_0^{\text{ref}} = 30 \text{ \AA}$ . The figure indicates that the core energies of aluminium very well satisfy Eqs. (2) and (3) for all character angles and core radii; this constitutes the major result of the

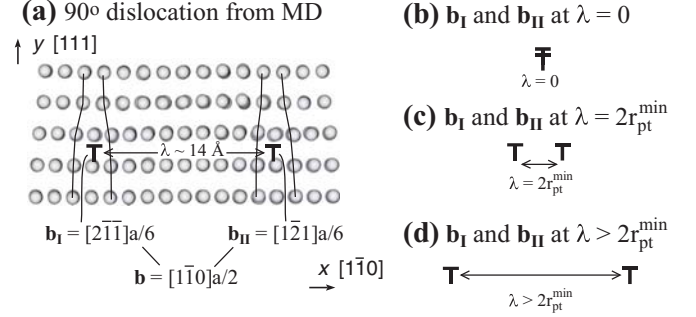


FIG. 6. Dissociated core configuration of a  $b = 90^\circ$  (edge) dislocation. (a) Front view of the MD configuration, (b) schematic of the perfect dislocation, (c) schematic of the two partials separated by  $r_{\text{pt}}^{\text{min}}$ , and (d) schematic of the two partials separated by  $\lambda$ .

present paper. We are currently implementing this finding in dislocation dynamics simulation models.

#### E. Effects of dislocation core structures

We have used elastic energy expressions for perfect dislocations to compute the core energy of a dislocation in a fcc solid that has dissociated into two partial dislocations bounding a stacking fault. Furthermore, we have found that the minimum core radius for this analysis is much smaller than the separation distance between these partial dislocations (shown below). With analysis of the core structure of an isolated dislocation, we can gain further insight into the physics of extended dislocation cores.

The front view ( $x$ - $y$ ) of the atomic configuration with  $\beta = 90^\circ$  (edge) dislocations is examined in Fig. 6(a). As expected, the perfect dislocation with a  $\vec{b} = [1\bar{1}0]a/2$  Burgers vector splits into two partials with Burgers vectors of  $\vec{b}_I = [2\bar{1}\bar{1}]a/6$  and  $\vec{b}_{II} = [1\bar{2}1]a/6$ . Because aluminium has a large stacking fault energy of  $\eta_{sf} = 133 \text{ mJ/m}^2$  [19], a relatively small separation distance of  $\lambda \approx 14 \text{ \AA}$  between the two partials is observed. However, this separation distance is significantly larger than the minimum core radius discovered above.

To better understand how the energetics of the dissociated structure relates to our results, we compute the energy change when a perfect edge dislocation dissociates into two partials (similar to the approach used in Ref. [27]). Since we are focusing on the core structure, we only consider an isolated extended dislocation in an infinite medium (rather than periodic arrays of dislocations, such as we did above). The line energy of a perfect edge dislocation in isotropic elasticity can be stated as [23]

$$\Gamma_{pf} = E_{c,pf}(r_{pf}, \beta = 90^\circ) + \frac{Gb^2}{4\pi(1-\nu)} \ln \frac{R}{r_{pf}}, \quad (4)$$

where the subscript  $pf$  denotes a perfect dislocation,  $E_{c,pf}(r_{pf}, \beta = 90^\circ)$  is the core energy associated with the core radius  $r_{pf}$ , and  $R$  is the outer cutoff radius. The energy change  $\Delta\Gamma$  when the two partials move apart is the work performed by the stress fields of the partials plus the energy of the stacking fault. To compute these quantities, we consider two stages of separation. First, the separation distance of the two partials



441 increases from  $\lambda = 0$  to  $\lambda = 2r_{pt}$  as shown in Fig. 6(c), where  
 442  $r_{pt}$  is the core radius of a partial dislocation so that  $2r_{pt}$  is  
 443 the overlap region of the two partial dislocation cores. During this  
 444 stage of separation we lump all of the work performed into a  
 445 change in the core energy, leading to an energy change in [18]

$$\Delta\Gamma_1 = (2E_{c,pt} + 2r_{pt}\eta_{sf}) - E_{c,pf}, \quad (5)$$

446 i.e., the core energy of the perfect dislocation  $E_{c,pf}$  is replaced  
 447 by the core energies of two partials  $2E_{c,pt}$  plus a stacking fault  
 448 energy ( $\eta_{sf}$  refers to the stacking fault energy per unit of area).  
 449 The work performed to further separate the two partials from  
 450  $\lambda = 2r_{pt}$  to  $\lambda > 2r_{pt}$  as shown in Figs. 6(c) and 6(d) can be  
 451 obtained from linear elasticity [18]. Adding in the energy from  
 452 the stacking fault then gives an energy change in

$$\Delta\Gamma_2 = \frac{Gb^2}{8\pi} \left( \frac{1}{3} - \frac{1}{1-\nu} \right) \ln \frac{\lambda}{2r_{pt}} + (\lambda - 2r_{pt})\eta_{sf}. \quad (6)$$

453 Hence, the total energy difference between the dissociated  
 454 dislocation Fig. 6(d) and the perfect dislocation Fig. 6(b) can  
 455 be expressed as

$$\begin{aligned} \Delta\Gamma &= \Delta\Gamma_1 + \Delta\Gamma_2 = 2E_{c,pt} - E_{c,pf} \\ &+ \frac{Gb^2}{8\pi} \left( \frac{1}{3} - \frac{1}{1-\nu} \right) \ln \frac{\lambda}{2r_{pt}} + \lambda\eta_{sf}. \end{aligned} \quad (7)$$

456 If we assume  $r_{pt} = 1.0$ ,  $b = 2.8634 \text{ \AA}$  and use the cor-  
 457 responding parameters mentioned above, the elastic and  
 458 stacking fault components give  $\frac{Gb^2}{8\pi} \left( \frac{1}{3} - \frac{1}{1-\nu} \right) \ln \frac{\lambda}{2r_{pt}} + \lambda\eta_{sf} =$   
 459  $-0.0345 \text{ eV/\AA}$ . The negative value drives the dissociation of  
 460 the perfect dislocation.

461 The total line energy of the extended dislocation is now  
 462  $\Gamma = \Gamma_{pf} + \Delta\Gamma$ . Using Eqs. (4) and (7) and after some  
 463 manipulation, we have that

$$\begin{aligned} \Gamma &= 2E_{c,pt} + \frac{Gb^2}{8\pi} \left[ \left( \frac{1}{3} - \frac{1}{1-\nu} \right) \ln \frac{\lambda}{2r_{pt}} + \frac{2}{1-\nu} \ln \frac{r_{pt}}{r_{pf}} \right] \\ &+ \lambda\eta_{sf} + \frac{Gb^2}{4\pi(1-\nu)} \ln \frac{R}{r_{pt}}. \end{aligned} \quad (8)$$

464 Only the last term contributes to the long-range elastic  
 465 component of the line energy, so we recognize that the core  
 466 energy we have computed and given in Table I corresponds to  
 467 the remaining terms,

$$\begin{aligned} E_c &= 2E_{c,pt} + \frac{Gb^2}{8\pi} \left[ \left( \frac{1}{3} - \frac{1}{1-\nu} \right) \ln \frac{\lambda}{2r_{pt}} + \frac{2}{1-\nu} \ln \frac{r_{pt}}{r_{pf}} \right] \\ &+ \lambda\eta_{sf}. \end{aligned} \quad (9)$$

468 This analysis demonstrates the connection between the line  
 469 energy expression for a perfect dislocation and the line energy  
 470 expression for an extended dislocation. Note that comparing  
 471 the long-range elastic interaction terms in Eqs. (4) and (8)  
 472 shows that  $r_{pf}$  is equivalent to  $r_{pt}$ , meaning that the minimum

473 core radius we have obtained with our atomistic computations  
 474 actually corresponds to the minimum core radius of the partial  
 dislocations rather than the overall extended dislocation. This  
 475 explains why we find a minimum core radius that is much  
 476 smaller than the separation distance between the partials.  
 477

#### IV. CONCLUSIONS

478 A robust MD model has been developed to calculate the  
 479 core energies of mixed dislocations. This model does not  
 480 require continuum boundary conditions, is applicable for the  
 481 full character angle range of  $0^\circ \leq \beta \leq 90^\circ$ , produces strongly  
 482 convergent results, and is constructed from orthorhombic  
 483 systems under the plane strain condition consistent with the  
 484 classical dislocation theories. Based on a high-fidelity bond  
 485 order potential, we have used this model to study dislocation  
 486 core energies of aluminium as a function of dislocation angle  
 487  $\beta$ . The following conclusions have been obtained:

488 (1) Although dislocations are dissociated, the apparent  
 489 (mathematical) dislocation core radius in aluminium is as small  
 490 as  $r_0 = 2.0 \text{ \AA}$  with isotropic elasticity theory and  $2.5 \text{ \AA}$  with  
 491 anisotropic elasticity theory, despite the fact that the extended  
 492 core has a width of greater than  $14 \text{ \AA}$ . This is because the core  
 493 radius pertains to the partial dislocations in the core.

494 (2) Values of  $r_0 > 2.0 \text{ \AA}$  can also be used. A larger radius in  
 495 general leads to a larger core energy. In particular, the increase  
 496 in core energy always equals the elastic strain energy of the  
 497 added volume due to the increase in the core radius.

498 (3) In isotropic elasticity theory, dislocation core energy  
 499 as a function of character angle satisfies an expression of  
 500 the form  $E_c(\beta) = A\sin^2\beta + B\cos^2\beta$ , which is similar to the  
 501 elastic energy.

502 (4) Dislocation energies are independent of temperature  
 503 over the temperature range considered here (100–300 K).  
 504

#### ACKNOWLEDGMENTS

505 Sandia National Laboratories is a multiprogram laboratory  
 506 managed and operated by Sandia Corporation, a wholly owned  
 507 subsidiary of Lockheed Martin Corporation, for the U.S.  
 508 Department of Energy's National Nuclear Security Adminis-  
 509 tration under Contract No. DE-AC04-94AL85000. This work  
 510 was performed under the Laboratory Directed Research and  
 511 Development (LDRD) Project No. 165724.  
 512

#### APPENDIX: DISLOCATION ENERGY UNDER PERIODIC BOUNDARY CONDITIONS

513 Following the previous approach for edge dislocations [18],  
 514 the dislocation line energy  $\Gamma$  for periodic mixed dislocations  
 515 with a mixed angle  $\beta$  can be derived as  
 516  
 517

$$\begin{aligned} \Gamma &= E_c + \frac{Gb^2}{4\pi(1-\nu)} \cos^2\alpha + \sin^2\beta E_{0,\text{edge}} + \cos^2\beta E_{0,\text{screw}} \\ &+ 2 \sin^2\beta \sum_{i=1}^{\infty} E_{i,\text{edge}} + 2 \cos^2\beta \sum_{i=1}^{\infty} E_{i,\text{screw}}, \end{aligned} \quad (A1)$$

where

$$E_{0,\text{edge}} = \frac{Gb^2}{4\pi(1-\nu)} \left\{ \ln\left(\frac{d}{r_0}\right) + \ln\left(\frac{L_y-d}{L_y}\right) - \ln\left[Ga\left(\frac{L_y+d}{L_y}\right)\right] - \ln\left[Ga\left(2-\frac{d}{L_y}\right)\right] \right\}, \quad (\text{A2})$$

$$E_{0,\text{screw}} = \frac{Gb^2}{4\pi} \left\{ \ln\left(\frac{d}{r_0}\right) + \ln\left(\frac{L_y-d}{L_y}\right) - \ln\left[Ga\left(\frac{L_y+d}{L_y}\right)\right] - \ln\left[Ga\left(2-\frac{d}{L_y}\right)\right] \right\}, \quad (\text{A3})$$

$$E_{i,\text{edge}} = \frac{Gb^2}{8\pi(1-\nu)} \left\{ \frac{4\pi i L_x \coth\left(\frac{\pi i L_x}{L_y}\right) \sin^2\left(\frac{\pi d}{L_y}\right)}{L_y \cosh\left(\frac{2\pi i L_x}{L_y}\right) - L_y \cos\left(\frac{2\pi d}{L_y}\right)} + \ln\left[\cos^2\left(\frac{\pi d}{L_y}\right) + \coth^2\left(\frac{\pi i L_x}{L_y}\right) \sin^2\left(\frac{\pi d}{L_y}\right)\right] \right\}, \quad (\text{A4})$$

$$E_{i,\text{screw}} = \frac{Gb^2}{8\pi} \ln\left[\cos^2\left(\frac{\pi d}{L_y}\right) + \coth^2\left(\frac{\pi i L_x}{L_y}\right) \sin^2\left(\frac{\pi d}{L_y}\right)\right]. \quad (\text{A5})$$

519 In Eqs. (A1)–(A5),  $E_c$  and  $r_0$  are the core energy and core  
 520 radius of an isolated dislocation,  $Ga$  is a Euler  $\gamma$  function,  $\coth$   
 521 and  $\cosh$  are hyperbolic functions,  $G$  is the shear modulus,  $\nu$   
 522 is Poisson’s ratio,  $b$  is Burgers magnitude, and  $\alpha$  is an angle  
 523 measuring the dislocation dipole direction (in particular,  $\alpha =$   
 524  $0^\circ$  means vertical dislocation dipole studied in the present  
 525 paper, and  $\alpha = 90^\circ$  means horizontal dislocation dipole). Note  
 526 that Eqs. (A1)–(A3) involve numerous changes compared to  
 527 the previous work [18]. First, the core radius  $r_0$  defined here  
 528 is equivalent to  $2r_0$  defined previously [18]. Second, there is  
 529 a constant  $\frac{Gb^2}{4\pi(1-\nu)} \cos^2\alpha$  in Eq. (A1) that is counted as elastic  
 530 contribution whereas in the previous work this constant term  
 531 is lumped into the core energy. These two modifications have  
 532 a zero impact on the model because they do not change the

total energy of dislocations; they only change the definition  
 of dislocation core radius and core energy. We modify these  
 definitions so that they are consistent with Hirth and Lothe  
 [25]. Finally, the second term in the curly braces “{ }” of  
 the right-hand side of Eqs. (A2) and (A3) is now expressed as  
 $\ln\left(\frac{L_y-d}{L_y}\right)$  whereas it was expressed as  $\ln\left(\frac{L_y-d}{L_y-2r_0}\right)$  in the previous  
 work [18]. The new expression is more rigorous, but the effect  
 is negligible because  $L_y \gg r_0$ .

Even Eq. (A1) does not have a closed form; it converges  
 very fast so that the error is negligible if a few terms (say 20)  
 are included (in the present paper, we included 100 terms).  
 We also wish to point out that Fourier methods can also be  
 used to compute the energies of dipolar dislocation arrays  
 [28,29].

[1] V. V. Bulatov and W. Cai, *Computer Simulations of Dislocations* (Oxford University Press, London, 2006).  
 [2] W. Cai, V. V. Bulatov, J. Chang, J. Li, and S. Yip, *Philos. Mag.* **83**, 539 (2003).  
 [3] W. Cai, V. V. Bulatov, J. Chang, J. Li, and S. Yip, *Phys. Rev. Lett.* **86**, 5727 (2001).  
 [4] J. Li, C. Z. Wang, J. P. Chang, W. Cai, V. V. Bulatov, K. M. Ho, and S. Yip, *Phys. Rev. B* **70**, 104113 (2004).  
 [5] M. Heggie, R. Jones, and A. Umerski, *Philos. Mag. A* **63**, 571 (1991).  
 [6] R. Jones, A. Umerski, P. Sitch, M. I. Heggie, and S. Öberg, *Phys. Status Solidi A* **137**, 389 (1993).  
 [7] A. S. Nandedkar and J. Narayan, *Philos. Mag. A* **61**, 873 (1990).  
 [8] U. Trinczek and H. Teichler, *Phys. Status Solidi A* **137**, 577 (1993).  
 [9] A. Aslanides and V. Pontikis, *Comput. Mater. Sci.* **10**, 401 (1998).  
 [10] J. R. K. Bigger, D. A. McInnes, A. P. Sutton, M. C. Payne, I. Stich, R. D. King-Smith, D. M. Bird, and L. J. Clarke, *Phys. Rev. Lett.* **69**, 2224 (1992).  
 [11] S. Ismail-Beigi and T. A. Arias, *Phys. Rev. Lett.* **84**, 1499 (2000).  
 [12] G. Wang, A. Strachan, T. Cagin, and W. A. Goddard III, *Phys. Rev. B* **67**, 140101(R) (2003).  
 [13] J. Bennetto, R. W. Nunes, and D. Vanderbilt, *Phys. Rev. Lett.* **79**, 245 (1997).  
 [14] N. Lehto and S. Öberg, *Phys. Rev. Lett.* **80**, 5568 (1998).  
 [15] X. Blase, K. Lin, A. Canning, S. G. Louie, and D. C. Chrzan, *Phys. Rev. Lett.* **84**, 5780 (2000).  
 [16] E. Clouet, L. Ventelon, and F. Willaime, *Phys. Rev. Lett.* **102**, 055502 (2009).  
 [17] G. Lua, N. Kioussis, V. V. Bulatov, and E. Kaxiras, *Mater. Sci. Eng., A* **309**, 142 (2001).  
 [18] X. W. Zhou, D. K. Ward, J. A. Zimmerman, J. L. Cruz-Campa, D. Zubia, J. E. Martin, and F. van Swol, *J. Mech. Phys. Solids* **91**, 265 (2016).  
 [19] X. W. Zhou, D. K. Ward, and M. E. Foster, *J. Alloys Compd.* **680**, 752 (2016).  
 [20] The MADSUM code is available at <http://micro.stanford.edu/~caiwei/Forum/2004-08-08-MadSum>  
 [21] S. Plimpton, *J. Comput. Phys.* **117**, 1 (1995).  
 [22] The LAMMPS download site [lammps.sandia.gov].  
 [23] A. H. Cottrell, *Dislocations and Plastic Flow in Crystals* (Oxford University Press, London, 1953).  
 [24] R. L. Norton, *Machine Design* (Pearson-Prentice Hall, Upper Saddle River, NJ, 2006).  
 [25] J. P. Hirth, and J. Lothe, *Theory of Dislocations* (McGraw-Hill, New York, 1968).  
 [26] V. Vitek, *Cryst. Lattice Defects* **5**, 1 (1974).  
 [27] T. Tsuru and D. C. Chrzan, *Sci. Rep.* **5**, 8793 (2015).  
 [28] T. Mura, *Proc. R. Soc. London, Ser. A* **280**, 528 (1964).  
 [29] M. S. Daw, *Comput. Mater. Sci.* **38**, 293 (2006).